An Exploration of 2D Coulomb Crystals in Quantum Computing

Robert T. Hackett
University of Washington, Department of Physics
Box 351560, Seattle, WA 98195-1560
(Dated: December 6, 2023)

In the nearly 20 years since Cirac and Zoller demonstrated that laser-cooled ions confined to a linear trap could be used to implement quantum gates, ion trapping has proven to be a suitable platform for practical quantum computation [1]. It didn't take long to show that each of the main DiVincenzo criteria (excluding those concerning flying qubits) can be satisfied by trapped ion systems, including single-qubit and multi-qubit gates [2]. Long trap lifetimes and internal-state coherence, along with strong interactions between ions, make it possible to achieve control and measurement with extremely high fidelity. At this point in time, the largest hurdle facing trapped ion quantum computing (and most other paradigms) is scalability, with some of the most advanced models being comprised of tens of qubits [3]. In this paper, I will explore the use of 2D Coulomb crystals of trapped ions for increasing the scale of future quantum processors [4, 5].

Keywords: trapped ion, Coulomb crystals, quantum computing

I. THE SPECTRUM OF TRAPPED IONS

The foundation of any quantum computer is the qubits. Physical qubits can take many forms, from superconducting circuits made of Josephson junctions to topological qubits—an interesting new approach that utilizes quasiparticle excitations known as anyons. Regardless of form, our concern is with two-level quantum systems in which one state of the qubit can be readily distinguished from the other. When examining trapped ions as a candidate qubit, we have a choice on what atom and isotope we use, and the various interactions within those atoms will lead to different forms of energy level splitting in the internal electronic states [2].

There are four primary domains on the spectrum of energy level splitting. Zeeman qubits (which utilize an applied field for splitting magnetic sublevels) have energy splitting on the order of tens of megahertz. Hyperfine qubits, which depend on the hyperfine energy levels of atoms arising from nucleus-electron interactions, have states separated by gigahertz, and are known for having long coherence times [6]. Fine structure qubits, separated by tens of terahertz, display energy splitting due to the electron spin and relativistic effects. Finally, there are optical qubits whose energy levels are separated by up to hundreds of terahertz. These have properties which are advantageous to long distance entanglement mediated by photons [7].

We'll take a look at at each of these categories in more detail to discuss the mechanisms which drive them, their respective strengths and weaknesses in general, and examine their potential applications within a 2D Coulomb crystal framework.

A. Zeeman Qubits

At the lower end of the energy splitting spectrum are Zeeman qubits. The isotopes chosen for this type of trapped-ion qubit are characterized as not having a nuclear spin. In this scenario, the two-level quantized states of the qubit are realized by the spin states of the ground state valence electron subject to an external magnetic field. We can do a quick calculation of the qubit resonance frequency, ω_{01}, in proportion to an external magnetic field, B_0

$$\frac{\omega_{01}}{2\pi} = \frac{\gamma_e}{2\pi}|B_0| \tag{1}$$

where we've used $\gamma_e/2\pi \approx 28\,\mathrm{GHz\,T^{-1}}$ as the electron gyromagnetic ratio. This tells us that Zeeman qubits,

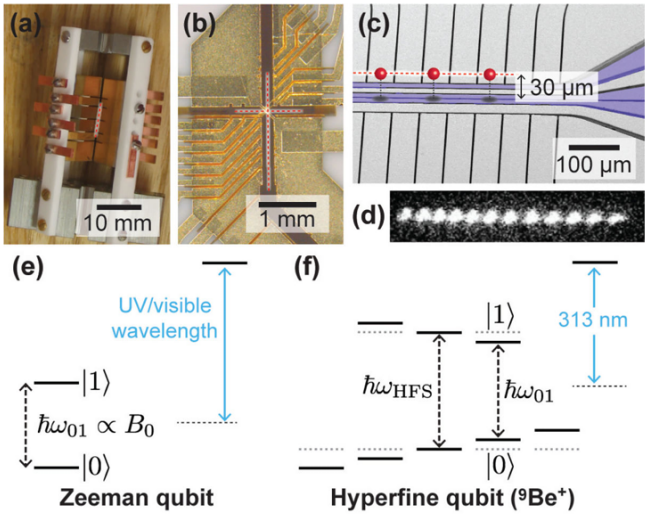

FIG. 1. (**a, b**) Two types of machined 3D traps. (**c**) Schematic of a surface-electrode trap. Shown in blue are integrated microwave antenna structures that allow for qubit control. The red spheres are ions, each in its own trapping potential well. (**d**) Real image of ions in a linear trap exhibiting fluorescence due to laser excitation. (**e, f**) Energy level diagrams comparing Zeeman qubit transitions to the closely related hyperfine qubit transitions. Figure borrowed from *Microwaves in Quantum Computing* [8]. Description is my own.

with frequencies of ∼10 MHz, can be operated in magnetic fields < 1 mT. As we'll see later, hyperfine qubits can also be operated in similarly small magnetic fields (but may require larger fields for higher-mass ions). Some ions which lend themselves to acting as Zeeman qubits are $^{174}Yb^+$ and $^{137}Ba^+$ [7, 9].

The low-frequency energy splitting, and subsequent weak magnetic field required to induce a transition, would seem to make Zeeman qubits sensitive to fluctuations in the magnetic field. That is indeed the case, and dephasing can occur for trapped ion qubits, and Zeeman qubits especially, due to deviations in the applied magnetic field. It can be shown that the first-order effects induce a shift in the frequency according to

$$\Delta\nu = \frac{g_s \mu_B}{\hbar} \Delta B \tag{2}$$

where $\Delta\nu$ and ΔB are the changes in frequency and magnetic field respectively, g_s is the Landé g-factor, μ_B is the Bohr magneton, and $\hbar$ is the reduced Planck constant. As such, magnetic field noise is a significant source of dephasing in Zeeman qubits, and the main disadvantage for using Zeeman qubits in quantum computing applications [8, 9].

However, even with that downside, Zeeman qubits offer the advantage of being resistant to leakage errors. Leakage occurs when a system contains additional states which are not used for the qubit states. Hyperfine qubits, for example, may be insensitive to first order magnetic fields, but they suffer from spontaneous scattering resulting from stimulated Raman processes that can lead to leakage (See Fig. 2). When dealing with quantum error correction, it becomes important to account for leakage out of the qubit subspace. In situations where the magnetic field can be sufficiently stabilized, ≤ 10 µG, it has been shown that Zeeman qubits exhibit a lower logical error rate when compared to similar hyperfine qubits [9].

B. Hyperfine Qubits

Moving up the scale, we encounter hyperfine qubits, which are characterized by the interaction between their valence electron spin and nuclear spin that produces a splitting in otherwise degenerate energy levels. For example, in the $^2S_{1/2}$ ground state, hyperfine splitting will produce two distinct energy levels corresponding to the difference in total angular momentum quantum number F.

Hyperfine qubits offer greater resistance to magnetic fields but at the cost of leakage into additional unwanted states. Similar ions can be used for hyperfine qubits as for Zeeman qubits, Yb^+ being a common example, where the difference in qubit type results from the different nuclear spins amongst different isotopes. This difference in spin is due to the number of nucleons. An even number of nucleons, each with spin 1/2, will pair off to give a total nuclear spin $I = 0$. However, in isotopes with an odd

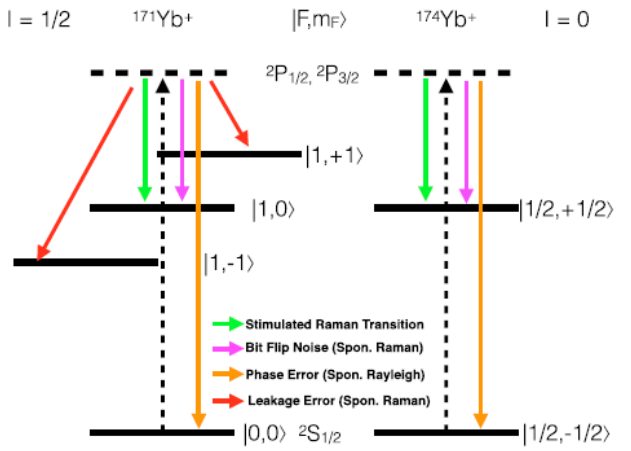

FIG. 2. Energy level diagram for $^{171}Yb^+$ and $^{174}Yb^+$ ions showing the potentials errors that can occur for each scattering event. These are assuming the ion always starts in a lower qubit state. Figured borrowed from *Comparing Zeeman qubits to hyperfine qubits in the context of the surface code: $^{174}Yb^+$ and $^{171}Yb^+$* [9]. Description is my own.

number of nucleons, the unpaired nucleon contributes a spin 1/2 so that odd-mass-number nuclei will have half-integer nuclear spin. For example, $^{174}Yb^+$ (used for Zeeman qubits) has a nuclear spin of $I = 0$, while $^{171}Yb^+$ has a nuclear spin of $I = 1/2$, making it a candidate for hyperfine qubits [9].

In general, the energy level splitting for hyperfine qubits will be in the low GHz range. For our example of $^{171}Yb^+$ the hyperfine splitting is 12.6 GHz. The magnetic fields used to manipulate ions in this regime are still considered relatively low with $B_0 \lesssim 50$ mT. Other odd isotopes that could be used for hyperfine qubits include $^{137}Ba^+$, which also benefits from long-lived metastable states and the longest visible-wavelength cooling transition of any potential ionic qubit [7]. In particular, there exist clock states $|F = 0, m_F = 0\rangle$ and $|F = 1, m_F = 0\rangle$ which are resistant to first-order magnetic fields. They only exhibit dependence on second-order magnetic fields, which can be derived from the Breit-Rabi formula

$$\Delta\nu = \frac{(g_j - g_I)^2 \mu_B^2}{2\hbar\omega} [2B_0 \Delta B + (\Delta B)^2] \tag{3}$$

where g_J and g_I are the electronic and nuclear Landé g-factors respectively, and ω is the angular frequency of the hyperfine splitting. It turns out, this second-order effect is negligibly small, so hyperfine qubits are not susceptible to magnetic field noise [2, 9].

The benefits that hyperfine qubits possess don't come without their share of drawbacks. The most prominent source of errors in hyperfine qubits is population leakage outside the qubit subspace. Our idealized qubit operates as a two-level system, however, there exist additional levels in the physical system beyond the two qubit states. If the ion leaks into one of these undesirable states, that

introduces errors. These types of errors are particularly harmful since standard error correction methods are not effective for treating them. There is research from Hayes *et al.* that shows leakage can be suppressed by pumping from the leakage state back into the qubit state by utilizing the quadrupole transition (see Fig. 3) [10].

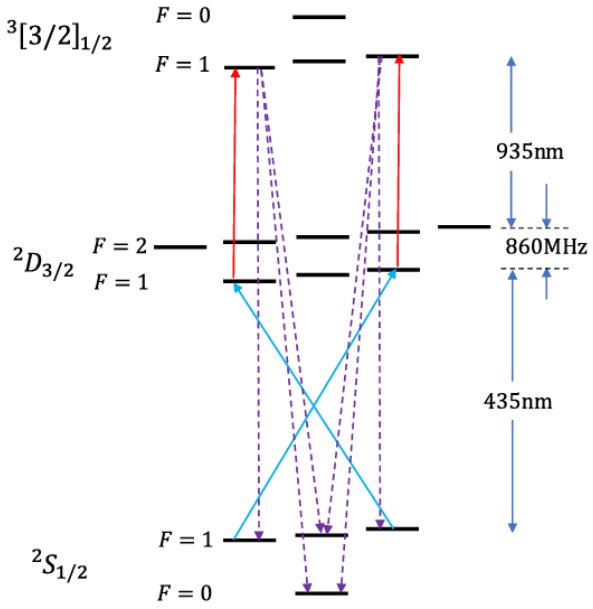

FIG. 3. Energy level diagram for $^{171}Yb^+$. In this repump scheme, leaked population is first driven to the $^2D_{3/2}$ by the 435 nm quadrupole transition. In the next step, the population is driven to $^3[3/2]_{1/2}$ by the 935 nm dipole transition. Completing the cycle, the $^3[3/2]_{1/2}$ states decay to $^2S_{1/2}$ with high probability. Figure borrowed from *Eliminating Leakage Errors in Hyperfine Qubits* [10]. Description is my own.

C. Fine Structure Qubits

Continuing through our spectrum of trapped ion qubits, we reach fine structure qubits, which operate in the range of $\lesssim 10$ THz. Similar to the hyperfine qubits we just discussed, fine structure qubits also suffer from leakage, and as a result, their lifetimes tend to be $\sim$ 1s. However, unlike hyperfine qubits, fine structure qubits fall into the category of zero nuclear spin qubits (along with Zeeman and optical qubits). As such, they typically come in the form of even mass number isotopes [2]. An example is $^{40}Ca^+$ which can transition between the metastable fine structure states $D_{3/2}$ and $D_{5/2}$ that are separated by 1.82 THz [11].

Stimulating these transitions for fine structure qubits is not much different from the previous qubits that we've discussed, except there are challenges that arise in generating narrow-linewidth laser beams at terahertz frequencies. One way around that is to utilize two phase-locked lasers in order to excite a stimulated Raman transition. For the $^{40}Ca^+$ ion, Toyoda *et al.* demonstrated that phase-locked Ti:sapphire lasers at 850 nm and 854 nm could be used to implement a CZ gate between the qubit states $|\uparrow\rangle \equiv |D_{5/2}(m_J = 1/2)\rangle$ and $|\downarrow\rangle \equiv |D_{3/2}(m_J = 1/2)\rangle$ in such a way (see Fig. 4) [11]. In this scheme, coherence times are potentially limited by the relative phase stability between the phase-locked laser. Nonetheless, the ease of scalability of IR lasers in integrated photonics offers a potential advantage over the blue and UV lasers required for Raman transitions in Zeeman and hyperfine qubits [2].

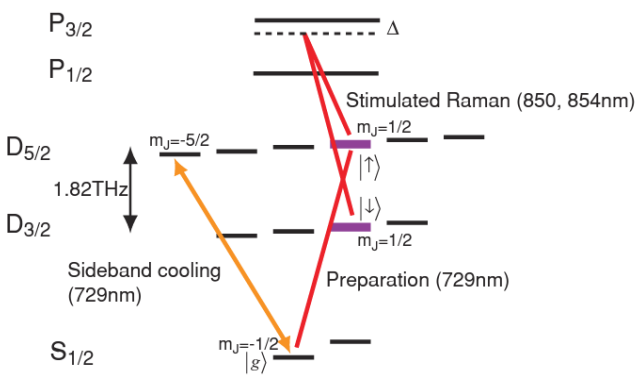

FIG. 4. Energy level diagram for $^{40}Ca^+$. The quadrupole transition between $S_{1/2}$ and $D_{5/2}$ is used to apply a conditional phase shift while the stimulated Raman transition is used to switch between qubit states $D_{5/2}$ and $D_{3/2}$, thereby implementing a CZ gate. Figure borrowed from *Quantum gate using qubit states separated by terahertz* [11]. Description is my own.

D. Optical Qubits

Finally, we reach our last stop on the energy splitting spectrum of trapped ions: optical qubits. Until now, all the previous qubit types have employed pairs of qubit states within the same orbitals. On the other hand, optical qubits generally make use of the ground-state S level and the metastable D level for the two qubit states. Typical energy level splitting is in the range of hundreds up to a thousand THz.

Being optically separated allows for extremely high efficiency detection of the qubit state based on resonant fluorescence. This works by utilizing an auxiliary level which rapidly decays to the ground state. First, a laser that is resonant with the transition between the S level ground state and the P level auxiliary state is applied to the qubit. If the qubit is in the ground state at that time, it will be excited to the P level, where, upon decay, it will emit a photon that can be detected. On the other hand, if the qubit is already in it's D level upper state, then it will not be in resonance with the applied laser

and the ion remains dark [2].

Optical qubits are generally similar to Zeeman and fine structure qubits when it comes to choice of isotope. It's possible to base an optical qubit on odd mass number isotopes (non-zero nuclear spin) but that can lead to unwanted shifts due to hyperfine splitting in the D state. Consequently, optical qubits will commonly make use of even mass number isotopes (zero-nuclear-spin). One such ion, $^{88}Sr^{+}$, has been shown to be a viable candidate for optical qubits capable of implementing a universal set of gates with high fidelity. As depicted in Fig. 5, the quantum information is encoded in states $\left|S_{1/2,\ \mathrm{m}=+1/2}\right\rangle$ and $\left|D_{5/2,\ \mathrm{m}=+3/2}\right\rangle$ [12].

This brings with it challenges related to the narrow line-widths required for the lasers used to control the optical transitions. Because fluctuations in the phase of the laser can lead to decoherence in the qubit, the lasers themselves can often become the limiting factor in coherence times [2]. In their scheme involving the $^{88}Sr^{+}$ qubit, Akerman *et al.* implemented stabilized diode lasers in a controller-follower configuration capable of producing a narrow linewidth. These diode lasers offer another advantage in that they tend to be affordable and compact compared with other light sources while still remaining capable of the precise frequencies necessary to facilitate quantum gate operations [12].

Optical qubits are being studied beyond just gate operations as well. The future of fault-tolerant quantum computation is likely to rely on quantum error correction (QEC) as devices increase in scale. QEC relies on being able to detect and correct errors during computation while keeping the encoded quantum information intact and unaltered. There are various platforms, including those making use of superconducting circuits and topological features, that have been presented as possible paths to achieve this. In their 2017 paper, Bermudez *et al.* examine how QEC could be implemented for trapped ions and chose to use $^{40}Ca^{+}$ ions due to the high-fidelity state detection that if offered by optical qubits (although their work shows the need for additional improvements before a truly beneficial QEC protocol can be achieved) [13].

II. TRAP GEOMETRY

Now that we have a better understanding of the types of ions used in trapped ion quantum computing, as well as some of the advantages and disadvantages they each have, we can turn our attention to the trapping configurations.

When considering the possible geometries that an ion trap can have, we're essentially given two choices: one-dimensional (1D), also known as linear arrays; or two-dimensional (2D), sometimes called planar arrays, which is the basis for the 2D Coulomb crystals we're building up to.

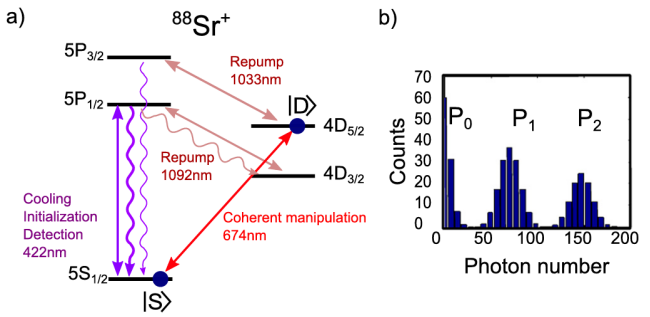

FIG. 5. (a) Energy level diagram for $^{88}Sr^{+}$. The transitions depicted with straight lines are driven by lasers, while the wavy lines indicate transitions due to spontaneous emission. The thick wavy line between the $^{5}P_{1/2} \rightarrow {}^{5}S_{1/2}$ transition represents the fluorescence used for detection. (b) Measurements of two-qubit fluorescence. Figure borrowed from *Universal gate-set for trapped-ion qubits using a narrow linewidth diode laser* [12]. Description is my own.

A. Linear Arrays

It may come as no surprise that the first quantum computers to be described using trapped ions made use of linear traps. Despite the simplistic geometry, all the necessary features of a quantum computer can be realized with linear ion traps. It's even possible to implement quantum gates between any set of ions in this scheme, not necessarily neighboring ions, for gates involving pairs, triplets, or any arbitrary number of ions. However, in practice, increasing the number of effective qubits is not an arbitrary task. Decoherence due to the environment interacting with the quantum system remains a significant challenge [1].

Nevertheless, advances have been made that show how quantum computers based on linear arrays could provide solutions to difficult problems in materials design and molecular modeling through quantum simulation. In one example from 2017, Zhang *et al.* successfully performed a quantum simulation of a dynamical phase transition (DPT) using up to 53 qubits in a linear ion trap. In this system, the qubits are coupled at long-range through their collective quantized motion due to Coulomb interactions. Each individual qubit is measured by a global long-range Ising interaction which has an efficiency of almost 99%. This high efficiency makes it possible to measure many-body correlations between qubits in one shot, thereby allowing the DPT to be probed directly [14].

The method employed by Zhang *et al.* for confinement of long ion chains relied on a three-layer linear Paul trap with $^{171}Yb^{+}$ ions. Across the chain, ion spacing is anisotropic, ranging from 1.5 µm at the center to 3.5 µm towards the ends. As one might expect, the average lifetime of the chain scales inversely with the number of ions. At the maximum, 53 ions, an average lifetime of about 5 minutes was observed (which was sufficient for this experiment). The greatest factor in limiting the effective

liftetime of the ion chain was Langevin collisions with residual background gas. When looking to scale up a system of this type, it will be crucial to implement cryogenic trap systems to reduce the pressure and collision energies [14].

More recently, a flexible scheme for maintaining efficient entanglement between ions in a long chain as the size scales up has been introduced by Leung and Brown. By utilizing both amplitude and frequency modulation, they show it's theoretically possible to apply high-fidelity pulse sequences to drive transverse motional modes, which can suppress gate errors (See Fig. 6). Those pulses in turn require greater power to operate, so there is a trade-off between higher tolerance against errors and power efficiency.

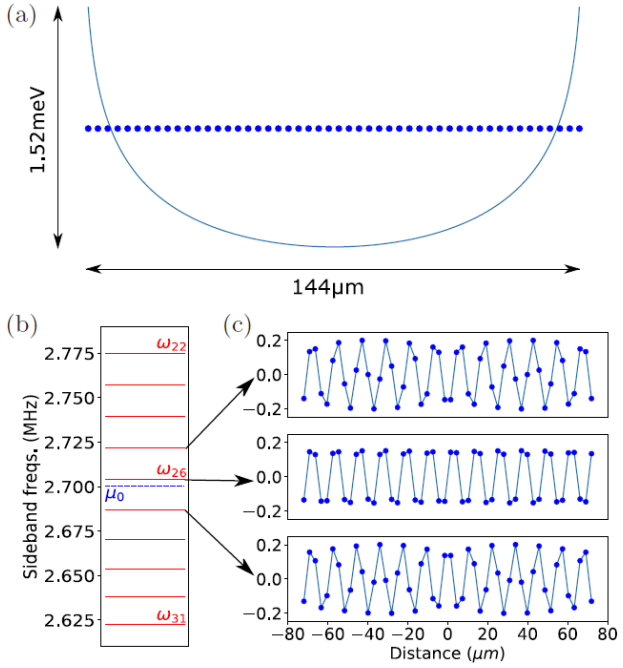

FIG. 6. (**a**) An idealized distribution of ions in a trap with $r = 0.95$. The minimum trap depth required to trap all 50 ions is 1.52 meV. (**b**) The middle band of the transverse motional frequencies. The approximate driving frequency is represented by the dashed blue line where $\mu_0 = \omega_{26} - 3.7\,\text{kHz}$. (**c**) The normalized 25th to 27th transverse motional modes. In the center is the 26th mode which exhibits a valuable uniformity making it an excellent candidate for two-qubit entanglement. Figure borrowed from *Entangling an arbitrary pair of qubits in a long ion crystal* [15]. Description is my own.

While linear arrays remain a promising area of research, there are some shortcomings to this particular trap geometry. In general, as the size of the ion chain increases, there is weaker motional coupling between ions with ion-ion coupling strength falling off as $1/s^{\alpha}$ where s is the distance between two ions. That then leads to limitations such as decreasing speed of qubit gates and a corresponding increase in noise-induced heating in the system (due to the gates taking longer) [2].

Those challenges could be overcome if the ion chain were to be broken into smaller pieces, or modules, which could perform operations at high-speed and efficacy within an individual module. That type of scheme would require some way of moving the quantum information between modules or even moving the ions themselves. This is possible given variable voltages in the ion trap electrodes that control the trapping potential. We can imagine breaking off subsets of ions from their modules and combining them in a new module to allow interaction. Then by returning them to their original positions, that quantum information has become more widely distributed. However, this process of splitting and joining many ion chains comes with it's own challenges and the ability to do it quickly and with high fidelity will be constrained by the size of the ion chain [2].

While distribution of quantum information is not impossible in a 1D linear array (and quantum computing is certainly possible), there are improvements that can be made in some areas by expanding to a 2-dimensional array (See Fig. 7).

B. Planar Arrays

When looking to scale up trapped-ion systems, 2D architectures have been proposed to mitigate the problems faced by larger linear arrays. In a linear chain, the ions are only weakly confined along the axial direction of the chain. Because of this, high heating rates can occur due to the axial motional modes making laser cooling a challenge. It also becomes a issue for laser-addressing the outer ions as the length of an ion chain grows. Just keeping a long one-dimensional chain in a linear form requires extremely anisotropic traps that ultimately limits how many ions can be controlled without introducing errors. Introducing a second spatial dimension can be shown to overcome these obstacles related to heating, quantum state manipulation, and more [5].

Having access to additional spatial dimensions also allows for the ability to simulate complex many-body systems. For example, the study of frustrated magnetic materials (where the natural tendency of magnetic moments to align with each other is hindered or frustrated by the geometric arrangement of atoms in the crystal lattice) becomes an intractable problem for classical computers when the number of spins becomes very large. A trapped-ion quantum simulator could be used to simulate lattice spin systems and even allow us to investigate the nonequilibrium quantum dynamics of the system [16].

Two-dimensional or planar arrays are built on much of the same concepts as the linear arrays we just discussed. There are various trapped-ion architectures that utilize 2D arrays including microtrap arrays, Penning traps, and multizone trap arrays. In general, Penning traps and microtraps have large ion separation which makes them ineffective for fast quantum gates that rely on the distance

dependent ion-qubit interaction. Penning traps also require fast rotation of the ion crystal which significantly increases the difficulty of individually addressing qubits [17].

For those reasons, Paul traps are preferred in many quantum computer applications. Paul traps can operate with lower magnetic fields, stationary 2D crystals, and facilitate individual addressing by laser beams. The main challenge in using Paul traps for producing 2D ion crystals comes from micromotion due to the oscillating applied electric field [18]. This type of driven motion is present in all radio-frequency (RF) ion traps, including 1D linear traps. However, micromotion can be minimized in the 1D case by placing the ions along the line corresponding to zero electric field amplitude. For 2D or even 3D cyrstals, the problem becomes more difficult and requires more sophisticated methods to mitigate the micromotion [19].

We can't say that 2D arrays are necessarily better than their 1D counterparts, but they do seem to be a promising path forward for scalable quantum technology. In the remainder of the paper, we'll take a closer look various platforms that utilize two-dimensional Coulomb crystals and how researchers are dealing with the challenges inherent in this architecture.

III. PAUL TRAPS

It's safe to say that Paul traps have proven their worth as a valuable tool for working with trapped ions. Even outside of quantum computing, experiments involving trapped ions have provided crucial insight to many fields of physics over the last few decades. For us in particular, Paul traps utilizing RF electric fields and stationary qubit arrays are the focus of much research involving 2D Coulomb crystals. Given that importance, we'll take this opportunity to examine the theory behind Paul traps and how they may be implemented experimentally.

A. Theoretical Framework

Studying the work of Leibfried *et al.*, we see a common model used to describe the electric potential $\Phi(x, y, z, t)$ of an RF trap [20]. This assumes a quadrupolar electrode layout, also known as point traps [2], and that the function for the potential can be decomposed into a time-independent (static) part and a time-dependent part that depends on the RF drive frequency ω_{RF} such that

$$\begin{aligned}\Phi(x, y, z, t) = U\frac{1}{2}(\alpha x^2 + \beta y^2 + \gamma z^2) \\ + \widetilde{U} cos(\omega_{RF} t)\frac{1}{2}(\alpha' x^2 + \beta' x^2 + \gamma' z^2).\end{aligned} \tag{4}$$

Taking into consideration that this potential needs to satisfy Laplace's equation at all times, we get conditions for the geometric factors

$$\begin{aligned}\alpha + \beta + \gamma = 0 \\ \alpha' + \beta' + \gamma' = 0.\end{aligned} \tag{5}$$

There are multiple choices of appropriate values here that define various confining fields. Of interest to us is the choice

$$\begin{aligned}-(\alpha + \beta) = \gamma > 0 \\ \alpha' = -\beta'\end{aligned} \tag{6}$$

which dynamically confines particles in the x-y plane and, at the same time, statically confines postively charged particles in the z-direction.

Ultimately, the interaction of ions and electromagnetic fields is quantum mechanical in nature (the motion of the trapped ions is quantized and closely approximated by static potential harmonic oscillators). However, a classical formulation can provide a decent approximation in many settings [20].

1. *Classical Equations of Motion*

For simplicity, we'll consider motion only in the x-direction, but these equations are readily applied to motion in other directions. Using the potential in eq. (4), the motion of a particle with mass m and charge $Z|e|$ is given by

$$\begin{aligned}\ddot{x} &= -\frac{Z|e|}{m}\frac{\partial \Phi}{\partial x} \\ &= -\frac{Z|e|}{m}\left[U\alpha + \widetilde{U}\cos(\omega_{RF} t \alpha')\right] x\end{aligned} \tag{7}$$

Using the substitutions

$$\xi = \frac{\omega_{RF} t}{2}, \quad a_x = \frac{4Z|e|U\alpha}{m\omega_{RF}^2}, \quad q_x = \frac{2Z|e|\widetilde{U}\alpha'}{m\omega_{RF}^2} \tag{8}$$

we can rewrite Eq. (7) in the form of the Mathieu equation

$$\frac{\mathrm{d}^2 x}{\mathrm{d}\xi^2} + [a_x - 2q_x \cos(2\xi)]x = 0 \tag{9}$$

which is a known differential equation with periodic coefficients and having stable solutions that can be found with the Floquet theorem [20].

For the sake of brevity, I'll leave out the complete derivation, but it suffices to say that the coefficients are recursively defined, and a numerical value must be extracted by truncating the continued fractions at the desired level of accuracy. The higher order contributions in the continued fraction typically fall off quickly for values of $a_x, q_x \ll 1$ in our region of interest [20].

What that work has done is allowed us to describe a region of stability in the potential field, and in particular,

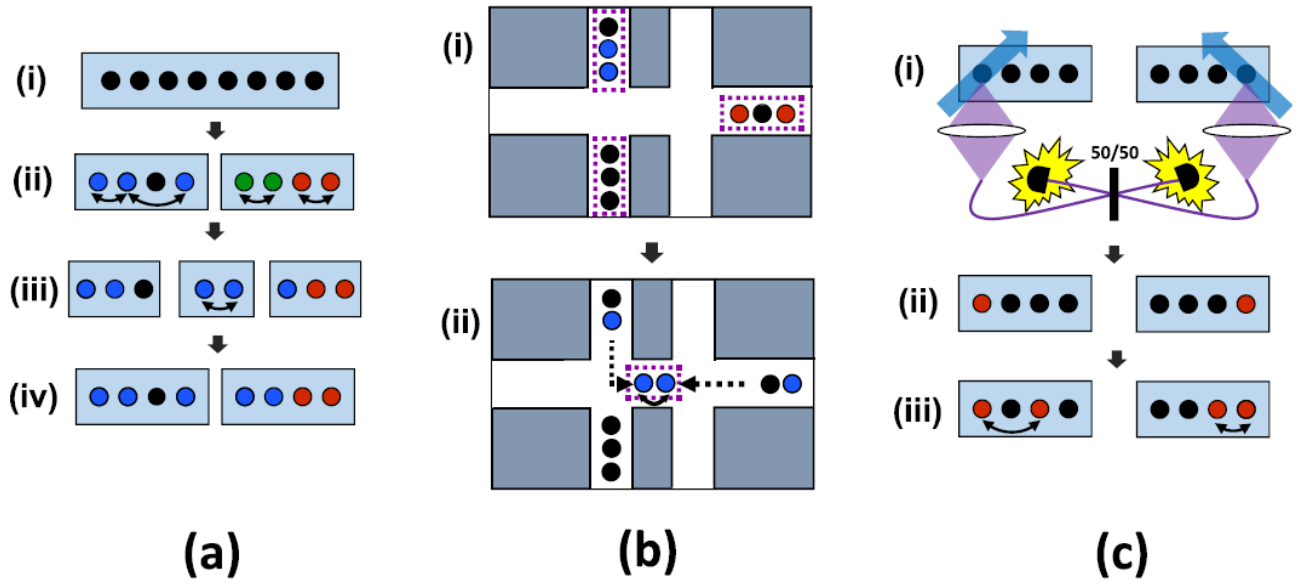

FIG. 7. Illustration of how entanglement can be achieved in various trapped-ion architectures. Black dots indicate no entanglement while like colors indicate entanglement between those ions. (**a**) Linear ion chain. (i) The qubits are initially in one long chain and no entanglment has ocurred. (ii) The chain is split into modules (blue boxes) where high-fidelity entangling gates can be performed. (iii) Ions from different modules are then combined in a new module where another entangling gate can be performed. (iv) The qubits are then returned to their original positions. (**b**) 2D array. (i) Qubits are separated into modules on a 2D array; they may or may not be entangled. They are kept in "memory zones" (dotted boxes) which are optimized for long coherence times. (ii) To entangle qubits from different modules, the ions are shuttled into an "interaction region" (dotted box) where entangling gates are performed. They are then shuttled back to their previous modules and the process can be repeated as needed. (**c**) Photonic interconnects. This example is of a linear array, but the concept can be applied to 2D arrays. (i) Each module contains a dedicated communication ion which is excited by a laser (blue arrows). The excited ions emit photons (purple) that are entangled with the internal ion state. The photons are directed through optics (ovals) into a 50/50 beam splitter where they interfere. (ii) If photons are simultaneously detected at the single-photon detectors (black hemispheres), that indicates the communication ions have been entangled. (iii) Intra-module entangling gates can then be performed to distribute the entanglement. Figure borrowed from *Trapped-ion quantum computing: Progress and challenges* [2]. Description is my own.

a lowest stability region—one which contains the point $(a_i, q_i) = (0, 0), \quad \forall\, i \in \{x, y, z\}$. The actual shape of the stability region still depends on the geometric factors α, β, and γ which themselves depend on the applied RF field and trap electrodes. Looking at Fig. 8(a) we see the lowest stability region of a Paul trap. β_i represent the borderlines of stability, and in the case of the cylindrically symmetric Paul trap, $\beta_x = \beta_y$. A similar situation occurs for the linear trap which has borderlines of stability mirrored over the q_x axis (Fig. 8(b)). In general, however, it's not imperative that RF traps have an intrinsic symmetry and the borderlines of stability in those cases may not have such simple relationships [20].

We can now approximate the motion of an ion in such a quadrupole potential. In the manner of Brownnutt *et al.* we get

$$x(t) = X_0 \cos(\omega_t t + \varphi_0)\left[1 + \frac{q_x}{2}\cos(\omega_{RF} t)\right] \tag{10}$$

where φ_0 is simply a phase that comes from initial conditions. Of more importance is ω_t and ω_{RF} which correspond to the "secular" motion and "micromotion" respectively. The secular, or trap, frequency ω_t is given by $\omega_t \approx \omega_{RF}/2$ and has a rather large amplitude that accounts for the bulk of the ion motion. The smaller motion, or micromotion, has a much smaller amplitude of $q_x/2$ that of the secular motion and oscillates at the drive frequency ω_{RF} [21].

To give us an idea of some typical numbers, in a trap with a potential $V \sim 500\,\mathrm{V}$ and ion-electrode spacing $d = 500\,\mu\mathrm{m}$, we'd expect to see $\omega_{RF} \sim 2\pi \times 20\,\mathrm{MHz}$ and $\omega_t \sim 2\pi \times 2\,\mathrm{MHz}$ [21].

This micromotion, as we've mentioned before, is detrimental to the successful operation of a quantum computer. Hence, it's of much importance to understand the entire picture when looking at motion of trapped ions.

2. *Quantum Mechanical Equations of Motion*

A more complete description of the motion of ions in an RF trap will require a quantum mechanical approach.

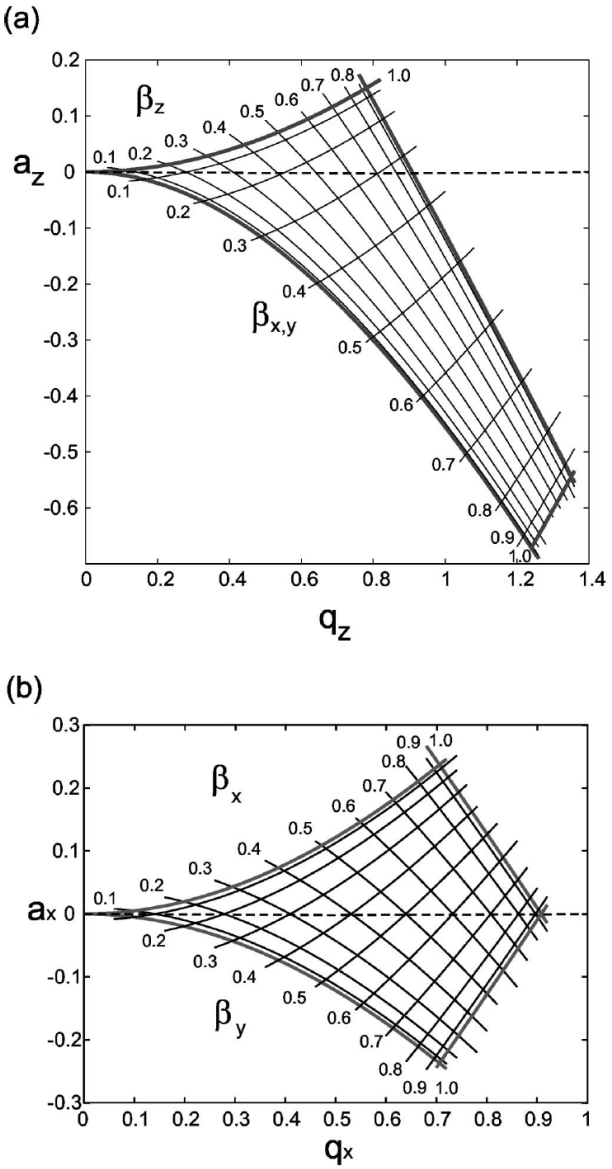

FIG. 8. (**a**) Stability diagram for a cylindrically symmetric RF trap. This is the case that $\alpha = \beta = -\gamma/2$ and $\alpha' = \beta' = -\gamma'/2$. Confinement is observed in all three axes. (**b**) For comparison, this is a stability diagram for a linear trap with $\alpha + \beta = -\gamma$, $\alpha' = -\beta'$, and $\gamma' = 0$. Figure borrowed and slightly modified from *Quantum dynamics of single trapped ions* [20]. Description is my own.

We again follow in the footsteps of Leibfried *et al.* and begin by writing the time-dependent potential $V(t)$ as

$$V(t) = \frac{m}{2} W(t)\hat{x}^2 \tag{11}$$

where $W(t)$ is treated like a time-varying spring constant and is given by

$$W(t) = \frac{\omega_{RF}^2}{4}[a_x + 2q_x \cos(\omega_R F t)]. \tag{12}$$

Using those equations, we can write the Hamiltonian of the motion, $\hat{H}^{(m)}$, which looks very similar to a static potential harmonic oscillator

$$\hat{H}^{(m)} = \frac{\hat{p}^2}{2m} + \frac{m}{2} W(t)\hat{x}^2. \tag{13}$$

Working directly off of Eq. (13) we get

$$\dot{\hat{x}} = \frac{1}{i\hbar}[\hat{x}, \hat{H}^{(m)}] = \frac{\hat{p}}{m} \tag{14}$$

$$\dot{\hat{p}} = \frac{1}{i\hbar}[\hat{p}, \hat{H}^{(m)}] = -mW(t)\hat{x} \tag{15}$$

which leads to

$$\ddot{\hat{x}} + W(t)\hat{x} = 0 \tag{16}$$

This is very similar to the Mathieu equation we found in Eq. (9). Enough so, that we can replace the operator $\hat{x}$ with a function $u(t)$ and it becomes possible to find solutions to Eq. (16) from the special solutions to the Mathieu equation with boundary conditions

$$u(0) = 1, \quad \dot{u}(0) = i\nu. \tag{17}$$

As before, I'll gloss over much of the derivation (leaving the reader free to explore *Quantum dynamics of single trapped ions* for themselves) [20] and arrive at the solution

$$\langle x'|n,t\rangle = \exp\left[-i\left(n + \frac{1}{2}\right)\nu t\right]\chi_n(t) \tag{18}$$

where $|n,t\rangle$ are a set of basis states for $n = 1, 2, ..., \infty$ and $\chi_n(t)$ is a complex function that includes, amongst other things, the classical micromotion term appearing as a pulsation in the wave function with the same period as the RF driving field.

B. Experimental Framework

Now that we've examined some of the theory behind the trapping potentials and the motion of trapped ions, we can take a closer look at some experimental setups involving 2D crystals of ions and Paul traps.

1. *Basic Structure*

The quadrupolar electrode layouts that we've discussed so far, also known as point traps, can be achieved in multiple ways as shown in Fig. 9.

Of greatest interest to our study of 2D Coulomb crystals are the surface, or planar, traps like those in Fig. 9(g). Planar traps of this variety create a pseudopotential minimum above the surface where ions can be held at distances of $\sim 100\,\mu$m from the electrode. By placing the electrodes in a single plane, we get the benefit of being

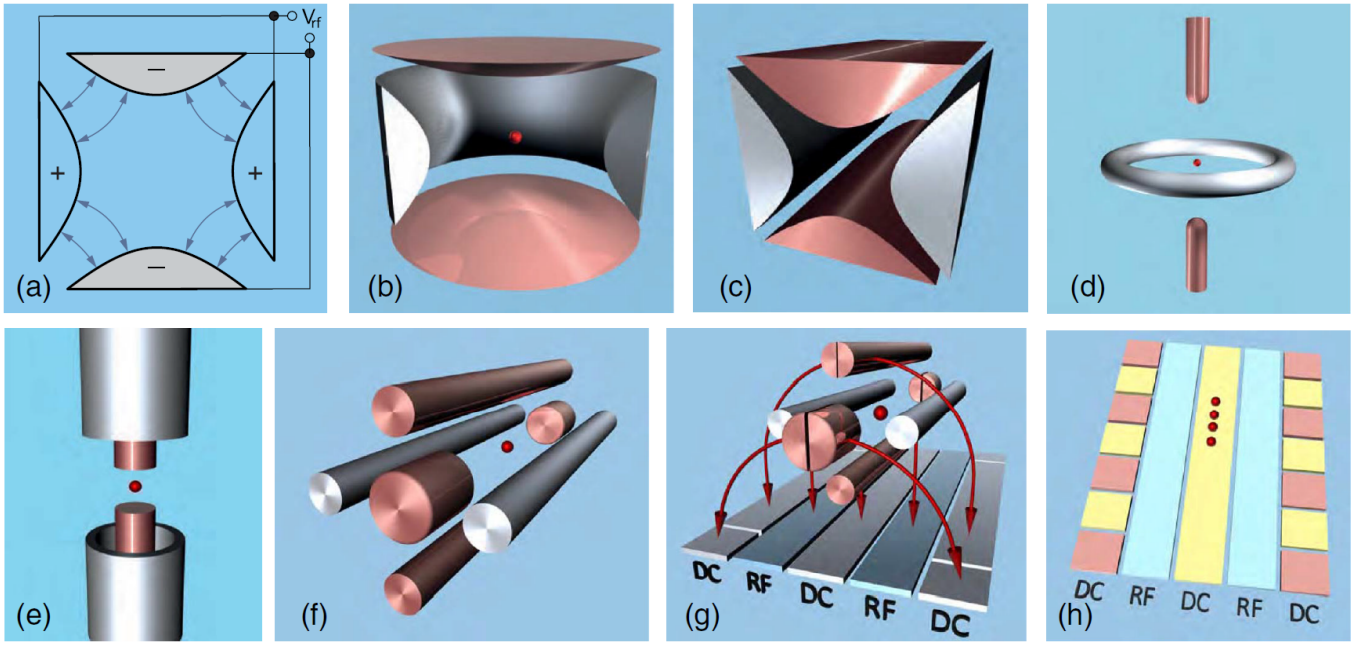

FIG. 9. Several possible trap configurations are seen here. (**a**) In the simplist case, a set of four perfectly hyperbolic electrodes create a perfectly quadrupolar field. (**b**) This is a basic ring trap. It has rotational symmetry and an create a pseudopotential capable of confining ions in three dimensions. (**c**) This is translationally symmetric and forms the basis for a linear trap. (**d**), (**e**) These are both topologically equivalent to the ring trap in (b). (**f**) This is topologically equivalent to the linear trap in (c) but with additional endcap electrodes making it a four-rod linear trap. (**g**) The four-rod trap in (f) can be reconstructed so that the electrodes are flattened into a single plane. This forms a linear "surface-electrode" trap. (**h**) A linear trap similar to (g) except the electrodes have been segmented to allow for multiple trapping zones. Figure borrowed from *Ion-trap measurements of electric-field noise near surfaces* [21]. Description is my own.

able to build them on chips, which would be an advantage for a scalable quantum computer. Even more useful still are the segmented traps seen in Fig. 9(h). With a point trap, it's not possible to place more than one ion at a point without increasing the undesirable micromotion. On the other hand, a segmented trap has separate, individually controlled segments allows for a single trap structure to contain multiple areas of potential minima that can hold an array of ions [2, 21].

These are only the most basic trapping configurations. In reality, because fields from stray charges or imperfect fabrication can result in excess micromotion, traps will often require additional compensation electrodes to minimize those effects. For most practical purposes, these are ignored when analyzing trap behavior, but quickly considered if analyzing noise in the system [21].

2. *Monolithic Traps*

Keeping the focus on surface traps for confining 2D Coulomb crystals, we'll take a look at some research involving monolithic traps. Monolithic traps are those where the components are integrated into a single piece, such as a microfabricated chip. Monolithic integration is expected to work in hand with modular approaches to manufacturing quantum technology. By combining chip-integrated components with a modular hierarchy, the hope is to realize scalability of quantum computers in a similar way to classical computers [2].

One such monolithic trap was implemented by Wang *et al.* in 2020 to demonstrate confinement of over 20 $^{171}Yb^{+}$ ions in a stationary 2D ion crystal [18]. Their monolithic trap is constructed from a single plate of alumina (Al_2O_3) coated in gold. The trap consists of 20 electrodes, of which 14 are connected to ground with the remaining electrodes connected to DC sources. What makes their setup unique is that the structure of the electrodes allows for precise control over the orientation of the 2D crystal plane. This makes it possible to rotate the principle axes of the trap potential, keeping the micromotions constrained to the 2D plane and perpendicular to the Raman laser beams. This has a significant impact on reducing the effect of micromotion on coherent quantum operations [18].

More recently, in 2023, work by Kiesenhofer *et al.* has demonstrated the ability to trap and control up to 105 $^{40}Ca^{+}$ ions in a monolithic RF trap designed specifically for quantum simulation [5]. In a standard Paul trap, there are two planes in which the ion crystal can be trapped: the plane spanned by two radial directions (see Fig. 10(a)), or the plane spanned by one radial direction and one axial direction (see Fig. 10(b)). In either case, in order to form a planar crystal, it's necessary for the ratio

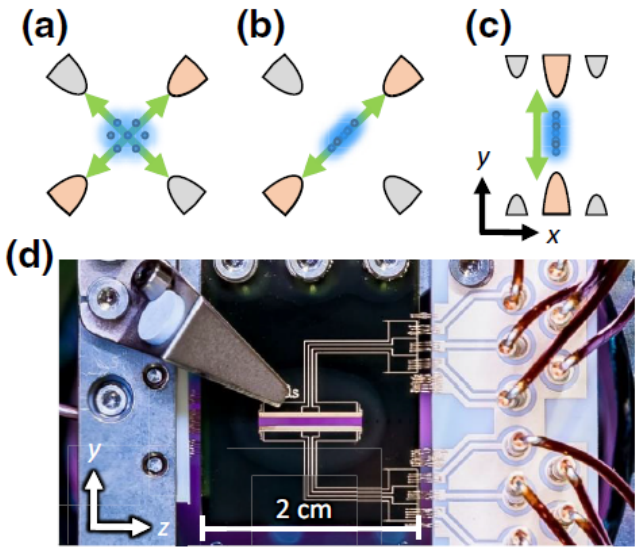

FIG. 10. (**a**), (**b**) Radial cross section of a Paul trap. The RF and DC electrodes are represented in orange and gray respectively. At the center of the electrodes is the ion crystal in blue. The green arrows represent the micromotions experienced by the ions. The ion crystal in (a) is oriented in the plane spanned by two radial direction. In (b) the crystal is oriented in the plane spanned by one radial direction and the axial direction. (**c**) This is a radial cross section of a three-layer trap. This configuration has the advantage of allowing optical access perpendicular to the micromotion. (**d**) A photograph of an ion trap in a vacuum chamber. The funnel aperture at the top left loads the ions from a calcium target. Figure borrowed and truncated from *Controlling Two-Dimensional Coulomb Crystals of More Than 100 Ions In A Monolithic Radio-Frequency Trap*. Description is my own.

of the secular frequency, ω_s, to the weak confinement frequency, ω_w, to obey the relationship $\omega_s/\omega_w > 1.23N^{1/4}$ where N is the number of ions. The secular frequency is in the direction of strong confinement, that is the direction in which the crystal is flattened, while the weak confinement is in the direction that the crystal extends.

Neither orientation in Fig. 10 has an advantage when it comes to RF-power requirements, however, the orientation in Fig. 10(b) only experiences driven micromotion along a single direction, which gives it an added benefit over the setup in Fig. 10(a). Building off of that, the three-layer trap in Fig. 10(c) maintains the beneficial crystal orientation while also giving optical access from directions perpendicular to the micromotion, allowing for laser cooling and laser addressing of individual ions. It's with this configuration that Kiesenhofer *et al.* were able to demonstrate trapping of 2D crystals of over 100 ions [5].

3. *Quantum Charge-Coupled Devices*

Among the variety of monolithic traps is a particular architecture known as a quantum charge-coupled device (QCCD). This is similar to the more common charge-coupled device (CCD) that's found in modern digital cameras. In the same way that a CCD stores imaging information as electrical charges that can be manipulated and moved around on the CCD, a quantum CCD contains separate regions that can hold and transport quantum information using dynamic electric fields [22]. Each of these different regions on the QCCD performs one of various functions such as loading, interaction, and measurement. The advantage of doing things that way is that it becomes easier to optimize that aspect of the trap for it's singular function [2].

Scientists studying QCCD architecture have shown in small scale trapped-ion experiments that error rates can be kept low, and they're hopeful that similar results can be achieved when scaling. Pino *et al.*, in 2021, introduced a scalable design for a cryogenic surface trap that integrates parallel interaction zones and fast ion transport into a QCCD foundation that could maintain the low error rates observed in individual ion crystals (see Fig. 11) [22].

QCCD architecture is promising, but it does face some challenges in creating a scalable quantum computer. Among other things, a succesful, scalable device, would need the ability to trap multiple small ion crystals, perform fast transport operations to move ions between crystals, and track qubit states across multiple zones. Each of those requirements can be met separately, but to combine those features into a single device presents a challenge. The device developed by Pino *et al.* is capable of meeting all those requirements and more, however, they do not predict that it will scale to thousands of qubits or more. Their QCCD device could be scaled by placing multiple chip-traps end to end, however, that linear scaling would also linearly increase the transport time between connected circuits, putting a damper on sustainable coherence. A future approach might look at maintaining better connectivity through photonic interconnects (using flying qubits), possibly even leverage different types of connectivity at different scales [22].

[1] J. I. Cirac and P. Zoller, Quantum computations with cold trapped ions, Phys. Rev. Lett. **74**, 4091 (1995).
[2] C. D. Bruzewicz, J. Chiaverini, R. McConnell, and J. M. Sage, Trapped-ion quantum computing: Progress and challenges, Applied Physics Reviews **6** (2019).
[3] S. A. Moses, C. H. Baldwin, M. S. Allman, R. Ancona, L. Ascarrunz, C. Barnes, J. Bartolotta, B. Bjork, P. Blanchard, M. Bohn, J. G. Bohnet, N. C. Brown, N. Q. Burdick, W. C. Burton, S. L. Campbell, J. P. C. I. au2, C. Carron, J. Chambers, J. W. Chan, Y. H.

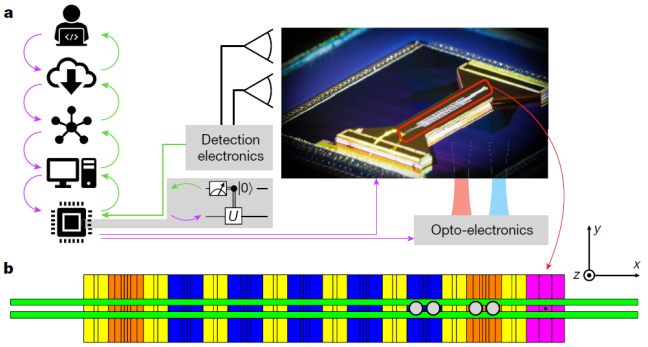

FIG. 11. (**a**) Left, a diagram of how information flows through the system: user, cloud, internal tasking, machine control, and field programmable gate array (FPGA). Right, a photopgrah of the QCCD trap. (**b**) Trap schematic. The long green wires are RF electrodes. Orange and blue are gate zones with yellow auxiliary zones in between. The gray circles indicate which gate zones were used in this work. Figured borrowed and truncated from *Demonstration of the trapped-ion quantum CCD computer architecture*. Description is my own.

Chen, A. Chernoguzov, E. Chertkov, J. Colina, J. P. Curtis, R. Daniel, M. DeCross, D. Deen, C. Delaney, J. M. Dreiling, C. T. Ertsgaard, J. Esposito, B. Estey, M. Fabrikant, C. Figgatt, C. Foltz, M. Foss-Feig, D. Francois, J. P. Gaebler, T. M. Gatterman, C. N. Gilbreth, J. Giles, E. Glynn, A. Hall, A. M. Hankin, A. Hansen, D. Hayes, B. Higashi, I. M. Hoffman, B. Horning, J. J. Hout, R. Jacobs, J. Johansen, L. Jones, J. Karcz, T. Klein, P. Lauria, P. Lee, D. Liefer, C. Lytle, S. T. Lu, D. Lucchetti, A. Malm, M. Matheny, B. Mathewson, K. Mayer, D. B. Miller, M. Mills, B. Neyenhuis, L. Nugent, S. Olson, J. Parks, G. N. Price, Z. Price, M. Pugh, A. Ransford, A. P. Reed, C. Roman, M. Rowe, C. Ryan-Anderson, S. Sanders, J. Sedlacek, P. Shevchuk, P. Siegfried, T. Skripka, B. Spaun, R. T. Sprenkle, R. P. Stutz, M. Swallows, R. I. Tobey, A. Tran, T. Tran, E. Vogt, C. Volin, J. Walker, A. M. Zolot, and J. M. Pino, A race track trapped-ion quantum processor (2023), arXiv:2305.03828 [quant-ph].

[4] A. Kato, A. Goel, R. Lee, Z. Ye, S. Karki, J. J. Liu, A. Nomerotski, and B. B. Blinov, Two-tone doppler cooling of radial two-dimensional crystals in a radio-frequency ion trap, Phys. Rev. A **105**, 023101 (2022).

[5] D. Kiesenhofer, H. Hainzer, A. Zhdanov, P. C. Holz, M. Bock, T. Ollikainen, and C. F. Roos, Controlling two-dimensional coulomb crystals of more than 100 ions in a monolithic radio-frequency trap, PRX Quantum **4**, 020317 (2023).

[6] U. Warring, C. Ospelkaus, Y. Colombe, R. Jördens, D. Leibfried, and D. J. Wineland, Individual-ion addressing with microwave field gradients, Phys. Rev. Lett. **110**, 173002 (2013).

[7] M. R. Dietrich, N. Kurz, T. Noel, G. Shu, and B. B. Blinov, Hyperfine and optical barium ion qubits, Phys. Rev. A **81**, 052328 (2010).

[8] J. C. Bardin, D. H. Slichter, and D. J. Reilly, Microwaves in quantum computing, IEEE journal of microwaves 10.1109/JMW.2020.3034071 (2021).

[9] N. C. Brown and K. R. Brown, Comparing zeeman qubits to hyperfine qubits in the context of the surface code: $^{174}Yb^{+}$ and $^{171}Yb^{+}$, Phys. Rev. A **97**, 052301 (2018).

[10] D. Hayes, D. Stack, B. Bjork, A. C. Potter, C. H. Baldwin, and R. P. Stutz, Eliminating leakage errors in hyperfine qubits, Physical review letters **124**, 170501 (2020).

[11] K. Toyoda, S. Haze, R. Yamazaki, and S. Urabe, Quantum gate using qubit states separated by terahertz, Phys. Rev. A **81**, 032322 (2010).

[12] N. Akerman, N. Navon, S. Kotler, Y. Glickman, and R. Ozeri, Universal gate-set for trapped-ion qubits using a narrow linewidth diode laser, New Journal of Physics **17**, 113060 (2015).

[13] A. Bermudez, X. Xu, R. Nigmatullin, J. O'Gorman, V. Negnevitsky, P. Schindler, T. Monz, U. G. Poschinger, C. Hempel, J. Home, F. Schmidt-Kaler, M. Biercuk, R. Blatt, S. Benjamin, and M. Müller, Assessing the progress of trapped-ion processors towards fault-tolerant quantum computation, Phys. Rev. X **7**, 041061 (2017).

[14] J. Zhang, G. Pagano, P. W. Hess, A. Kyprianidis, P. Becker, H. Kaplan, A. V. Gorshkov, Z.-X. Gong, and C. Monroe, Observation of a many-body dynamical phase transition with a 53-qubit quantum simulator, Nature **551**, 601 (2017).

[15] P. H. Leung and K. R. Brown, Entangling an arbitrary pair of qubits in a long ion crystal, Phys. Rev. A **98**, 032318 (2018).

[16] B. Yoshimura, M. Stork, D. Dadic, W. C. Campbell, and J. K. Freericks, Creation of two-dimensional coulomb crystals of ions in oblate paul traps for quantum simulations, EPJ Quantum Technology **2**, 2 (2015).

[17] S.-T. Wang, C. Shen, and L.-M. Duan, Quantum computation under micromotion in a planar ion crystal, Scientific Reports **5**, 8555 (2015).

[18] Y. Wang, M. Qiao, Z. Cai, K. Zhang, N. Jin, P. Wang, W. Chen, C. Luan, B. Du, H. Wang, Y. Song, D. Yum, and K. Kim, Coherently manipulated 2d ion crystal in a monolithic paul trap, Advanced Quantum Technologies **3**, 2000068 (2020), https://onlinelibrary.wiley.com/doi/pdf/10.1002/qute.202000068.

[19] A. Kato, A. Nomerotski, and B. B. Blinov, Micromotion-synchronized pulsed doppler cooling of trapped ions, Phys. Rev. A **107**, 023116 (2023).

[20] D. Leibfried, R. Blatt, C. Monroe, and D. Wineland, Quantum dynamics of single trapped ions, Rev. Mod. Phys. **75**, 281 (2003).

[21] M. Brownnutt, M. Kumph, P. Rabl, and R. Blatt, Ion-trap measurements of electric-field noise near surfaces, Rev. Mod. Phys. **87**, 1419 (2015).

[22] J. M. Pino, J. M. Dreiling, C. Figgatt, J. P. Gaebler, S. A. Moses, M. S. Allman, C. H. Baldwin, M. Foss-Feig, D. Hayes, K. Mayer, C. Ryan-Anderson, and B. Neyenhuis, Demonstration of the trapped-ion quantum ccd computer architecture, Nature **592**, 209 (2021).